

Effects of flexoelectricity and weak anchoring on a Fredericksz transition cell

E. Mema, L. Kondic, and L. J. Cummings

*Department of Mathematical Sciences and Center for Applied Mathematics and Statistics
and New Jersey Institute of Technology, Newark, New Jersey 07102, USA*

(Received 7 September 2016; published 5 January 2017)

We consider a mathematical model that consists of a nematic liquid crystal layer sandwiched between two parallel bounding plates, across which an external field is applied. We investigate how the number and type of solutions for the director orientation within the layer change as the field strength, anchoring conditions, and material properties of the nematic liquid crystal layer vary. In particular, we focus on how the inclusion of flexoelectric effects alters the Fredericksz and saturation thresholds.

DOI: [10.1103/PhysRevE.95.012701](https://doi.org/10.1103/PhysRevE.95.012701)

I. INTRODUCTION

Over the past several decades, liquid crystals (LCs) and in particular nematic liquid crystals (NLCs) have emerged as important industrial materials due primarily to increased production of electronic devices using liquid crystal displays (LCDs) [1]. A typical LCD device consists of millions of pixels, each made of a NLC layer confined between two parallel plates, and crossed polarizers. The plane of polarized light passing through the layer may be rotated, to a degree that depends on the orientation of the NLC molecules within the layer. The molecular orientation is in turn controlled by the boundary conditions at the plates (the preferred orientation of molecules at the boundaries, known as *anchoring*) as well as the external forces (usually an applied electric field). The basic operating principle of a conventional LCD is that the plane of the polarized light is differently rotated in the “field on” and “field off” states, hence, the two states appear optically distinct when viewed through the second polarizer.

NLCs typically consist of rodlike molecules, which have a dipole moment. An electric field can affect the molecular orientation within an NLC layer via two mechanisms. Applying an electric field causes the NLC molecules to align parallel or perpendicular to the electric field direction according to the orientation of their dipole moment. If the dipole moment is parallel to the long molecular axis, then the molecules align parallel to the electric field; in contrast, if it is perpendicular to the long axis, then they will align perpendicular to the electric field [2]. In addition to this “dielectric effect,” the asymmetric nature of the molecules induces a distortion in the form of molecular splay and bend, the so-called “flexoelectric effect” [3,4].

The effect of an applied external field on a confined NLC layer has been widely investigated and the *Fredericksz transition* phenomenon has been well understood for many years now [2,5–7]. A Fredericksz transition cell consists of a NLC layer bounded between two parallel plates where an electric field is applied in a direction perpendicular to the layer. It is observed that in the presence of strong planar anchoring, the nematic director field (representing the local average molecular orientation) aligns parallel to the bounding plates throughout the entire layer, when the applied field strength is low. As the applied field increases past a critical value (known as the *Fredericksz threshold*), a new director configuration, which aligns partially with the applied field in

the interior of the layer while respecting the strong planar anchoring at the boundaries, is favored energetically [2].

In the presence of weak planar surface anchoring, the same observations hold initially as the field is increased. However, now as the electric field is increased further still, a second critical value, known as the *saturation threshold*, is reached: this is the magnitude of the applied field at which the director aligns fully with the electric field direction, breaking the anchoring of the director at the surfaces [8,9]. This is also often called the *weak Fredericksz transition*. In this scenario, three steady-state director configurations exist: (i) the director aligns parallel to the anchoring orientation at the boundary (the “horizontal” solution for which anchoring dominates); (ii) the director aligns parallel to the electric field (the “vertical” solution for which the electric field dominates); and (iii) the director adopts a nontrivial solution for which there is a balance between surface anchoring and electric field effects.

The classical Fredericksz transition cell model accounts for the dielectric effect of the applied field but neglects flexoelectric effects, and assumes strong planar anchoring at the cell boundaries. This is the setup considered by most authors, with a few notable exceptions. Brown and Mottram considered the effects of flexoelectricity on a Fredericksz cell above the Fredericksz transition [6]. A theoretical investigation carried out by Derzhanski *et al.* [7] studies the effect of flexoelectricity and surface polarization on a Fredericksz transition cell as a weak electric field is applied (the applied voltage considered is strong enough to induce a deformation in the director field across the layer, i.e., past the Fredericksz threshold, but deformations are assumed to remain small so that the equation governing the director angle is linearized). Four different geometries are considered: (a) a homeotropic layer (director field is homeotropic throughout the layer in the absence of an electric field) with an electric field applied parallel to the bounding substrates (parallel electric field), (b) a homeotropic layer with an electric field applied perpendicular to the bounding substrates (perpendicular electric field), (c) a planar layer (director field is planar in the absence of an electric field) with parallel electric field, and (d) a planar layer with perpendicular electric field. Each case is expanded to include positive and negative dielectric anisotropy and different anchoring strength at each boundary (16 total cases considered), but always in the linear deformation regime. In each case, the authors study the effects of flexoelectricity and

surface polarization and how each of them affect the director configurations.

In this paper, we consider a setup similar to case (d) in [7], i.e., a Freedericksz transition cell where an electric field is applied perpendicular to the NLC layer, which has positive dielectric anisotropy. We account for both dielectric and flexoelectric contributions to the free energy, with anchoring of arbitrary strength at both bounding surfaces. We investigate how the inclusion of flexoelectricity affects not only the Freedericksz threshold, but also the saturation threshold, via a dimensionless material parameter that measures the ratio of flexoelectric and elastic effects. We also consider systematically the effect of anchoring strength on the results, and study how even small changes of the anchoring conditions can change the outcome dramatically. Where applicable, we interpret and compare our results with those obtained by Derzhanski *et al.* in [7]. While our approach is mainly numerical (necessitated by the fact that we consider arbitrary electric field strength so the director governing equation is nonlinear), we complement our study with some analytical results.

Our previous related work has focused on two specific issues of relevance to LCDs. First, we have studied how anchoring conditions may be tuned to permit *bistability*, the existence of two (optically) distinct stable states in the absence of an applied electric field, in a prototype LCD, using a model very similar to that considered here [10–12]. Bistability in LCDs is important since it offers potential for considerable energy savings: a device can maintain its display configuration without drawing power. When the display needs to be changed, individual pixels can be switched to the alternative stable state by transient application of an electric field. Second, we have studied the electric field nonuniformities that can arise in a confined NLC layer across which a voltage is applied [13]. Most investigations of electric field effects within such NLC layers assume a uniform field, whereas in reality the NLC and field interact, leading to gradients in the field. This paper is concerned primarily with investigating the bifurcations between distinct solution types; determining how bifurcation thresholds are affected by material properties of the system; and in some cases how bifurcations may be destroyed altogether by small changes in anchoring conditions. The relevance of our earlier work to this study will be discussed later, in particular in Sec. III where our simulations enter regimes in which the uniform field assumption may not be valid and in Sec. V where we discuss the regime such that changes in the anchoring conditions can induce bistability.

The paper is laid out as follows: In Sec. II we present the mathematical model and discuss its nondimensionalization, leading to the key dimensionless parameters for the system. In Sec. III we outline our solution scheme, present selected numerical results, focusing on the effect of flexoelectricity on the director solution and how our results compare with the predictions outlined in [7]. In Sec. IV we explore how flexoelectricity affects the Freedericksz and saturation thresholds in a Freedericksz transition cell while Sec. V briefly explores how changes in the anchoring conditions affect the results. In our investigation, we pay particular attention to the stability of each director configuration, augmenting our numerical results with analytical techniques such as the calculus of variations, and

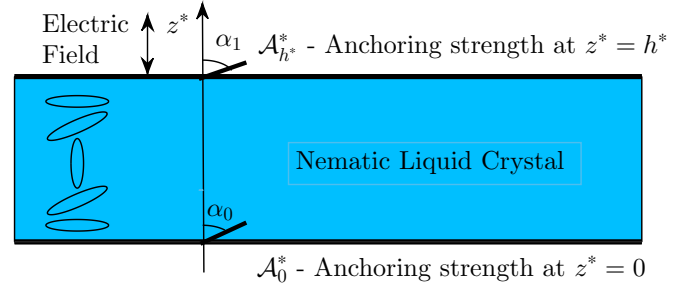


FIG. 1. Sketch showing the setup and summarizing the key parameters in dimensional coordinates.

linear stability analysis (LSA), as described in the Appendix. Section VI summarizes our conclusions.

II. MATHEMATICAL MODEL

We consider a layer of nematic liquid crystal of thickness h^* , placed between two parallel bounding surfaces at $z^* = 0$ and h^* as shown in Fig. 1. The local average molecular orientation throughout the layer is described by a unit vector director field n , which we assume lies in the (x^*, z^*) plane, with its properties varying in the z^* direction only. Hence, we consider a one-dimensional model where the director is expressed in terms of a single angle $\theta(z^*) \in (-\pi/2, \pi/2]$, the angle the director makes with the z^* axis: $n = (\sin \theta, 0, \cos \theta)$. We assume that an electric field $E^* = E^*(0, 0, 1)$ is applied in the z^* direction, perpendicular to the bounding plates. The generated field is assumed to be uniform everywhere as if the field were applied *in vacuo*. In reality, the molecules of the NLC layer contain electric dipoles that interact with the applied field, causing it to deviate from its uniform state. However, we have shown in prior work [13] that the uniform field approximation is good under certain conditions, which we will discuss later after outlining our model and associated parameters.

The mathematical model is based on the Ericksen-Leslie continuum theory for nematics where the total energy density of a liquid crystal layer comprises bulk and surface energy densities, that are functions of the director orientation n . To simplify the model, we make the common assumption that the bend and splay elastic constants are equal in magnitude. In the presence of a uniform electric field, the bulk energy density consists of the elastic, dielectric, and flexoelectric contributions W_e^*, W_d^*, W_f^* [2, 14, 15] given by

$$2W_e^* = K^* \{(\nabla^* \cdot n)^2 + [(\nabla^* \times n) \times n]^2\}, \quad (1)$$

$$2W_d^* = -\varepsilon_0^*(\varepsilon_{\parallel} - \varepsilon_{\perp})(n \cdot E^*)^2, \quad (2)$$

$$W_f^* = -E^* \cdot [e_1^*(\nabla^* \cdot n)n + e_3^*(\nabla^* \times n) \times n], \quad (3)$$

where K^* is the single elastic constant for the NLC, $\varepsilon_0^* = 8.854 \times 10^{-12} \text{ C}^2 \text{ N}^{-1} \text{ m}^{-2}$ is the permittivity of free space, and ε_{\parallel} and ε_{\perp} are the relative dielectric permittivities parallel and perpendicular to the long axis of the nematic molecules. The flexoelectric effect typically arises because NLC molecules possess shape asymmetry [4, 16]. When they align in an electric

field, therefore, distortions may be induced. For example, if molecules are slightly pear shaped, being fatter at one end than the other, then when all the “pears” align in a field a splay distortion will be induced due to the fat ends occupying more space than the thin ends. Similarly, if molecules are slightly banana shaped, and all the “bananas” align in an electric field, then a net bend distortion results. Flexoelectricity is also possible in symmetric polar liquid crystals such as 5CB. In this case, polar liquid crystals tend to form dimers with antiparallel alignment between molecular dipoles. In the presence of an electric field, the alignment is not completely antiparallel leading to a net polarization. This polarization couples to a bend and splay deformation [4,16]. We note that the flexoelectric coefficients used in this paper are imported from experimental literature [4] and account for both dipolar and quadrupolar flexoelectricity.

It has been observed that the effect of flexoelectricity in a weakly anchored NLC layer is closely related to surface polarization [7,17]. In fact, these two effects are so tightly bound that substantial errors in the flexoelectric coefficients may be induced when trying to separate the two effects in experiments [7,18]. Surface polarization can arise as a result of the asymmetric nature of the NLC molecules and their interaction with the substrate molecules or as a result of the spatial dependence of the nematic order parameter in a thin layer close to an interface [18–21]. Although our study does not explicitly account for surface polarization, it has been shown [20] that these effects can easily be incorporated into the present framework. Specifically, they may be included by modifying the coefficient of the flexoelectric term in the boundary conditions [upcoming Eqs. (6a)–(6c)]. Our results may therefore be considered to cover surface polarization effects also, at least in the symmetric anchoring cases considered for the majority of this paper.

The total free energy of the system J^* (per unit area of bounding plates) is given as follows:

$$J^* = \int_0^{h^*} W^* dz^* + g_0^*|_{z^*=0} + g_{h^*}^*|_{z^*=h^*}, \quad (4)$$

where $g_{\{0,h^*\}}^*$ are the surface anchoring energies at boundaries $z^* = 0, h^*$ and, under the assumptions outlined above, $W^* = W_e^* + W_d^* + W_f^*$ simplifies to

$$W^* = \frac{K^*}{2} \theta_{z^*}^2 - \frac{E^{*2} \varepsilon_0^* (\varepsilon_{\parallel} - \varepsilon_{\perp})}{2} \cos^2 \theta + \frac{E^* (e_1^* + e_3^*)}{2} \theta_{z^*} \sin 2\theta, \quad (5)$$

where the subscript $(\cdot)_{z^*}$ denotes the derivative: $\partial/\partial z^*$. For the surface energy contributions, we use the Rapini-Papoular form [22] $g_{\{0,h^*\}}^* = (\mathcal{A}_{\{0,h^*\}}^*/2) \sin^2(\theta - \alpha_{\{0,h^*\}})$, where $\alpha_{\{0,h^*\}}$ are the preferred anchoring angles at $z^* = 0, h^*$, respectively, and $\mathcal{A}_{\{0,h^*\}}^*$ are the associated anchoring strengths. From a formal mathematical viewpoint, surface anchoring is strong if the molecules at each surface align exactly with the preferred anchoring angles at the corresponding surfaces; and it is weak if the molecules deviate from the preferred orientation. Strictly speaking, therefore, strong anchoring is achieved only in the limit $\mathcal{A}^* \rightarrow \infty$.

We follow several authors (e.g., Kedney and Leslie [23], Davidson and Mottram [24], Cummings *et al.* [11]) in assuming that the system evolves as a gradient flow to its total free energy minimum. This process can be represented as follows:

$$\begin{aligned} & \langle \mu^* \theta_{t^*}, \eta \rangle + \langle W_{\theta}^*, \eta \rangle + \langle W_{\theta_{z^*}}^*, \eta_{z^*} \rangle + [\tilde{\nu}^* \eta \theta_{t^*} + \eta g_{h^* \theta}^*]|_{z^*=h^*} \\ & + [\eta \tilde{\nu}^* \theta_{t^*} + \eta g_{0\theta}^*]|_{z^*=0} = 0, \end{aligned}$$

where $\langle A, B \rangle = \int_0^{h^*} AB dz^*$, the parameter η is a sufficiently smooth test function, and the parameters μ^* and $\tilde{\nu}^*$ represent the bulk and surface rotational viscosities associated with the NLC molecules (see [11,23,24]; for consistency we use the same notation as our earlier work [11]). Integration by parts leads to the following evolution equation and boundary conditions:

$$\mu^* \theta_{t^*} = K^* \theta_{z^* z^*} - \frac{\varepsilon_0^* (\varepsilon_{\parallel} - \varepsilon_{\perp}) E^{*2}}{2} \sin 2\theta, \quad (6a)$$

$$\begin{aligned} \tilde{\nu}^* \theta_{t^*} &= K^* \theta_{z^*} - \frac{\mathcal{A}_0^*}{2} \sin 2(\theta - \alpha_0) \\ &+ \frac{E^* (e_1^* + e_3^*)}{2} \sin 2\theta \Big|_{z^*=0}, \end{aligned} \quad (6b)$$

$$\begin{aligned} -\tilde{\nu}^* \theta_{t^*} &= K^* \theta_{z^*} + \frac{\mathcal{A}_{h^*}^*}{2} \sin 2(\theta - \alpha_{h^*}) \\ &+ \frac{E^* (e_1^* + e_3^*)}{2} \sin 2\theta \Big|_{z^*=h^*}. \end{aligned} \quad (6c)$$

We nondimensionalize Eqs. (5)–(6c) as follows:

$$\begin{aligned} z &= \frac{z^*}{h^*}, \quad t = \frac{t^* K^*}{\tilde{\mu}^* h^{*2}}, \quad W = \frac{h^{*2} W^*}{K^*}, \\ g_{\{0,1\}} &= \frac{g_{\{0,h^*\}}^* h^*}{K^*}, \quad \mathcal{A}_{\{0,1\}} = \frac{h^* \mathcal{A}_{\{0,h^*\}}^*}{K^*} \end{aligned} \quad (7)$$

(W plays an important role in the calculus of variations approach used in the Appendix), obtaining the following dimensionless boundary value problem:

$$\theta_t = \theta_{zz} - \mathcal{D} \sin 2\theta, \quad (8a)$$

$$\tilde{\nu} \theta_t = \theta_z - \frac{\mathcal{A}_0}{2} \sin 2(\theta - \alpha_0) + \frac{\mathcal{F}}{2} \sin 2\theta \quad \text{on } z = 0, \quad (8b)$$

$$-\tilde{\nu} \theta_t = \theta_z + \frac{\mathcal{A}_1}{2} \sin 2(\theta - \alpha_1) + \frac{\mathcal{F}}{2} \sin 2\theta \quad \text{on } z = 1, \quad (8c)$$

where $\tilde{\nu} = \tilde{\nu}^*/(\mu^* h^*)$ represents the dimensionless surface viscosity and \mathcal{D} and \mathcal{F} represent the relative strengths of dielectric anisotropy and elasticity and of flexoelectricity and elasticity, respectively:

$$\mathcal{D} = \frac{h^{*2} E^{*2} \varepsilon_0^* (\varepsilon_{\parallel} - \varepsilon_{\perp})}{2K^*}, \quad \mathcal{F} = \frac{h^* E^* (e_1^* + e_3^*)}{K^*}. \quad (9)$$

We consider the common case in which the molecules align parallel to the direction of the electric field, rather than perpendicular to it (i.e., $\varepsilon_{\parallel} - \varepsilon_{\perp} > 0$), so $\mathcal{D} > 0$ always in our model. The parameter \mathcal{F} can change sign, if the electric field direction is reversed. We note that if surface polarization is taken into account, the governing equations [Eqs. (8a)–(8c)] remain unchanged and we only need to modify the value of

\mathcal{F} in the boundary conditions as shown in Ref. [20]. In the following, however, for clarity and to keep the discussion focused, we will refer only to flexoelectric effects when considering the influence of the parameter \mathcal{F} on results. The ratio $\Upsilon = \mathcal{F}^2/\mathcal{D}$ is independent of the applied electric field:

$$\Upsilon = \frac{2(e_1^* + e_3^*)^2}{K^* \varepsilon_0^* (\varepsilon_{\parallel} - \varepsilon_{\perp})}. \quad (10)$$

Υ is thus a material parameter of the liquid crystal layer, independent of cell design and constant for a specific liquid crystal material.

With characteristic values of $h^* \sim 1\text{--}20 \mu\text{m}$, $E^* \sim 1 \text{ V } \mu\text{m}^{-1}$, $K^* = 8 \times 10^{-12} \text{ N}$, $e_1^* + e_3^* \sim 5 \times 10^{-12} \text{ Cm}^{-1}$ – $280 \times 10^{-12} \text{ Cm}^{-1}$, and $\varepsilon_{\parallel} - \varepsilon_{\perp} \sim 5$ [4], the dimensionless parameters \mathcal{F} and \mathcal{D} can take a wide range of values [$|\mathcal{F}| \in (5, 125)$ and $\mathcal{D} \in (2, 1100)$]. Consistently with this range of values, in Sec. III, we fix $|\mathcal{F}|$ and \mathcal{D} and vary the anchoring strength and field direction [$\text{sign}(\mathcal{F})$] to determine the influence on the director configuration throughout the layer. In Sec. IV, we vary Υ (and inherently \mathcal{F}) while keeping $\mathcal{D} = 10$ to explore how flexoelectricity affects the Freedericksz and saturation thresholds.

The presentation so far assumes a uniform electric field, but in reality the applied field interacts with the NLC leading to some nonuniformity. Cummings *et al.* [13] studied the validity of the uniform field approximation in our model. They concluded that the approximation is valid in the large field limit, when $|\mathcal{F}| \gg 1$ [with $\Upsilon, \mathcal{A}_0, \mathcal{A}_1 \sim o(|\mathcal{F}|)$] as well as the small field limit (with $\Upsilon \sim |\mathcal{F}| \ll 1$ and $\Upsilon^{-1} \sim |\mathcal{F}| \ll 1$). In the latter case, the director does not feel the nonlinearity that arises in the electric potential due to the small field strength. Caution should, however, be exercised in using the uniform field approximation in the case where $\Upsilon \gg 1$ (strong flexoelectric effect) and $|\mathcal{F}| = O(1)$. We present simulation results both in the regime where the uniform approximation is valid and where it may not be. For the latter cases, we note that some corrections to the results may be needed.

The parameters $\mathcal{A}_{\{0,1\}}$ in Eqs. (8) represent the dimensionless anchoring strength at each boundary. In experiments, typical values for strong anchoring hover around $\mathcal{A}^* \sim 10^{-3} \text{ Jm}^{-2}$ while $\mathcal{A}^* \sim 10^{-5}\text{--}10^{-6} \text{ Jm}^{-2}$ for weak anchoring [25]. Depending on the thickness of the NLC layer, $\mathcal{A}_{\{0,1\}}$ can take a wide range of values $\mathcal{A}_{\{0,1\}} \in (125, 2500)$ (strong anchoring) and $\mathcal{A}_{\{0,1\}} \in (0.125, 25)$ (weak anchoring). Consistently with this range of values, in our simulations we use $\mathcal{A}_{\{0,1\}} = 0.1, 1, 5, 10, 20$ to represent weak anchoring and $\mathcal{A}_{\{0,1\}} = 1000$ for strong anchoring. For most of our work here, we consider the case where anchoring is planar at both boundaries, $\alpha_{\{0,1\}} = \pi/2$, with equal anchoring strengths ($\mathcal{A}_0 = \mathcal{A}_1$). This symmetry guarantees monostability (only one stable director configuration for a given electric field strength). In cases where asymmetry is introduced (through anchoring angles), the system can be bistable, admitting two nontrivial director configurations $\theta_{n,1}$ and $\theta_{n,2}$ [10,11]; such cases are briefly considered in Sec. VB.

In the following sections, we use numerical and analytical methods to determine and investigate solutions to the boundary value problem given by Eqs. (8) for various electric field strengths accounting for both dielectric and flexoelectric

contributions. In particular, we focus on how the stability of each director solution changes with the electric field strength, and with the material parameter Υ , which characterizes the strength of flexoelectricity relative to elasticity. We also extend our investigation to determine the influence of variations in the anchoring strength and angles at the boundaries in both monostable and bistable systems.

III. SOLUTION SCHEME AND NUMERICAL RESULTS

We begin by illustrating some key features of the director configurations in the classical case where the anchoring at each boundary is planar ($\alpha_{\{0,1\}} = \pi/2$) and the layer is subjected to an applied perpendicular electric field. Both “strong” and “weak” anchoring are considered. We note that the effect of flexoelectricity for planar (weak and strong anchoring) angles has been previously investigated [6,7]. Here, we extend those results to include the effect of flexoelectricity not only on the Freedericksz threshold, but also on the saturation threshold (arbitrary electric field strength). In addition, we consider systems with different anchoring orientations (e.g., the nearly planar anchoring case and the hybrid aligned case), and investigate the structure of each system as the electric field strength varies. In our numerical simulations, we solve the boundary value problem given by Eqs. (8) using the Crank-Nicolson discretization scheme for the linear parts of the equations. Nonlinear terms are treated explicitly using the forward Euler discretization scheme [26]. A grid size $\Delta z = 10^{-3}$ and $\Delta t = 10^{-4}$ is found sufficient to produce accurate results in all cases considered.

Except where explicitly stated otherwise, the initial condition on all of our simulations is taken as $\theta(z, 0) = \pi z/4$. We note, however, that except for some simulations of Sec. VB (where asymmetric anchoring conditions may lead to bistability), all scenarios considered are monostable, and the final state reached is independent of the initial condition used. Figure 2 shows the evolution of the director field in time for two cases: (i) when no electric field is applied across the layer, (ii) when an electric field of moderate strength characterized by $|\mathcal{F}| = 5$ and $\mathcal{D} = 25$ is applied. Strong and weak planar anchoring represented by $\mathcal{A}_{\{0,1\}} = 1000$ [Fig. 2(a)] and $\mathcal{A}_{\{0,1\}} = 5$ [Figs. 2(b) and 2(c)], with $\alpha_{\{0,1\}} = \pi/2$, are considered; for both cases we observe that, in the absence of an electric field, the director evolution is driven purely by the anchoring angles, hence, we obtain a director solution that is parallel to the bounding plates [$\theta(z, t) = \pi/2$] throughout the domain (black horizontal lines). In the presence of an electric field, however, the molecules should tend to align parallel to the electric field direction since $\mathcal{D} > 0$.

Consistently with our expectations and with the results of [6], we observe that for a strongly anchored system [Fig. 2(a)], the director aligns nearly parallel to the applied field in the interior of the layer and nearly parallel to the walls close to the boundaries [see red lines in Fig. 2(a)]. Although our model includes both dielectric and flexoelectric contributions, flexoelectric deformations are not observed here (as noted also by Derzhanski *et al.* [7]). Flexoelectricity is dominated by the surface anchoring in this strongly anchored case. This may also be seen from the boundary conditions (8b) and (8c), which are the only place in the model where

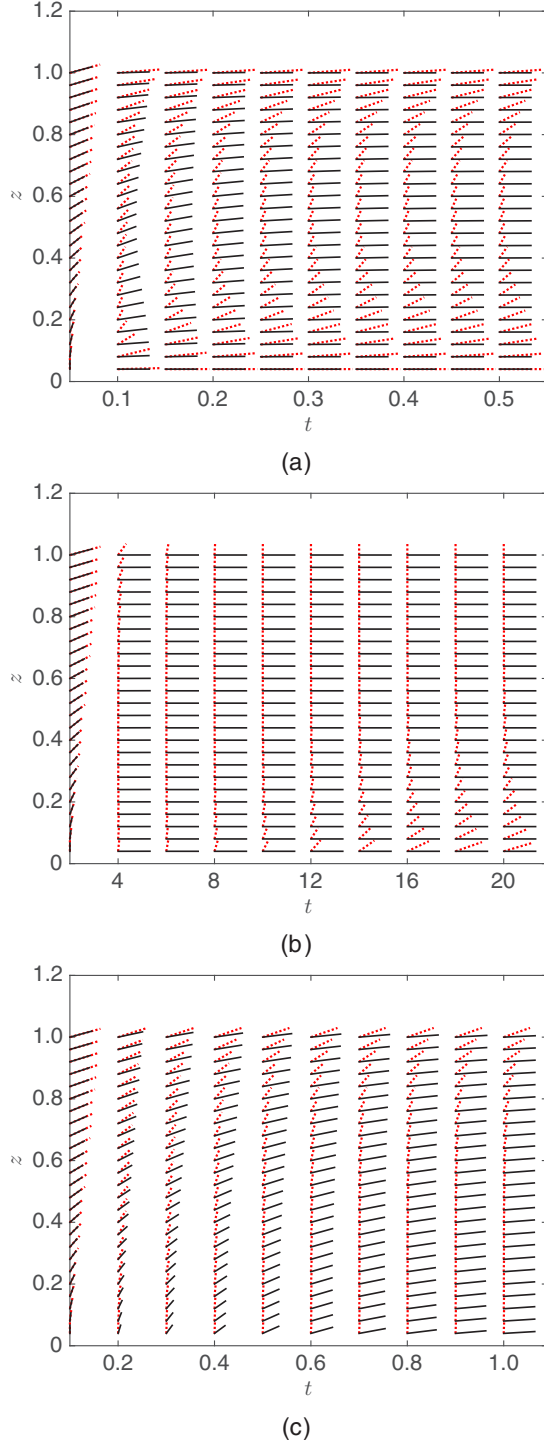


FIG. 2. Evolution of director field in time for $\alpha_{\{0,1\}} = \pi/2$, with (a) $\mathcal{A}_{\{0,1\}} = 1000$ (strong anchoring), $\mathcal{F} = 5$, and $\mathcal{D} = 25$, (b) $\mathcal{A}_{\{0,1\}} = 5$ (weak anchoring), $\mathcal{F} = 5$, and $\mathcal{D} = 25$ and (c) $\mathcal{A}_{\{0,1\}} = 5$, $\mathcal{F} = -5$, and $\mathcal{D} = 25$. All figures show the director evolution in dimensionless time when no electric field is applied $\mathcal{D} = \mathcal{F} = 0$ (black solid lines) and when an electric field of strength $\mathcal{F} = \pm 5$ and $\mathcal{D} = 25$ is applied (red dotted lines).

the flexoelectricity parameter \mathcal{F} and the surface anchoring strengths $\mathcal{A}_{\{0,1\}}$ appear. These boundary conditions suggest that it is the ratio of these two parameters that is key in determining whether flexoelectricity significantly affects the

system behavior. Consistent with [6], we also note from these conditions that, in the symmetric anchoring case considered here ($\mathcal{A}_0 = \mathcal{A}_1$, $\alpha_{\{0,1\}} = \pi/2$), if $\mathcal{F} = 0$, we anticipate symmetry about the layer's centerline $z = 0.5$, but asymmetry when $\mathcal{F} \neq 0$. As the anchoring strength \mathcal{A} increases for fixed \mathcal{F} , we would therefore expect that the director configuration observed becomes increasingly symmetric about $z = 0.5$, and this is borne out by Fig. 2(a), where $\mathcal{F} = 5$ and $\mathcal{A}_{\{0,1\}} = 1000$: the director configuration shown in this figure is almost exactly the same as in the Freedericksz transition cell where the flexoelectric effects are neglected and anchoring is strong [6] (and would be identical to the results of [6] in the formal limit $\mathcal{A}_{\{0,1\}} \rightarrow \infty$).

For the weakly anchored system ($\mathcal{A}_{\{0,1\}} = 5$) shown in Figs. 2(b) and 2(c), however, we observe significant asymmetry about the cell centerline: with an electric field of strength $\mathcal{F} = 5$, $\mathcal{D} = 25$, the molecules align parallel to the electric field at the upper boundary $z = 1$ as well as in the interior [see red lines in Fig. 2(b)]. This is a consequence of the asymmetric nature of the molecules discussed earlier which is reflected in the flexoelectric free energy density [see Eq. (3)]. Due to the weak anchoring conditions, the flexoelectric distortion plays an important role in the director alignment and hence in the response to the electric field [3,7,27]. The direction of the electric field dictates the sign of \mathcal{F} . Figure 2(c) confirms our expectations that if the sign of \mathcal{F} is reversed, then the director profile is simply reflected about the line $z = 0.5$.

For this simple monostable case of symmetric, planar, surface anchoring ($\alpha_0 = \alpha_1 = \pi/2$ and $\mathcal{A}_0 = \mathcal{A}_1$) we next investigate how flexoelectricity changes the steady-state molecular orientation of the NLC layer with weak planar anchoring ($\alpha_{\{0,1\}} = \pi/2$, $\mathcal{A}_{\{0,1\}} = 5$), when an electric field, above the Freedericksz threshold but below the saturation threshold, is applied in the z direction. Neglecting flexoelectricity [$\mathcal{F} = 0$ in Eqs. (8)], but accounting for the weak anchoring, Ref. [8] has shown that a director solution symmetric about $z = 0.5$ is the minimum free energy solution. To study the effects of flexoelectricity, we vary the material parameter Υ [given by Eq. (10)] while keeping \mathcal{D} fixed and observe how the director configuration changes as Υ (and inherently \mathcal{F}) is increased. Figure 3 shows the steady-state director profiles obtained at large times after solving Eqs. (8) for different values of Υ . When $\Upsilon = 0$ (black solid curve), we recover the results of Ref. [8] for weak anchoring but no flexoelectricity. The molecules align nearly parallel to the electric field direction in the interior of the layer while at the boundaries there is a tradeoff between the weak planar anchoring and the field-aligning dielectric effect. As Υ increases (strong flexoelectric effect), the molecules will splay and bend causing the director to align almost parallel to the electric field in the bulk and at the upper boundary. Note that $\Upsilon = 10$ falls under the case where $\Upsilon \gg 1$ and $\mathcal{F} = \mathcal{O}(1)$, where the uniform field assumption may not be valid [13]. However, assuming that the director solution we calculate here for $\Upsilon = 10$ is not significantly different than that for the true nonuniform field case, we conclude that flexoelectricity plays an important role in the alignment of liquid crystal molecules in the presence of an electric field and it affects the Freedericksz and saturation thresholds.

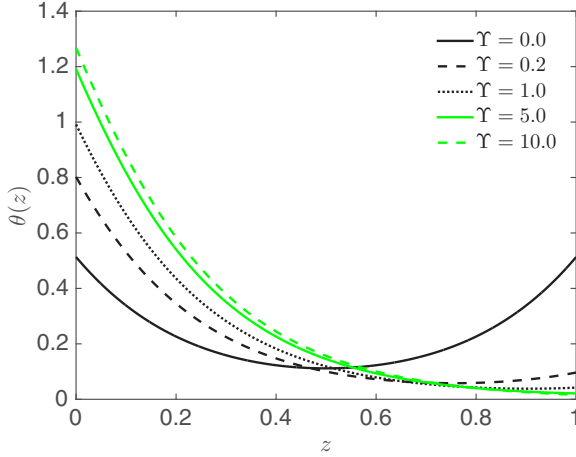


FIG. 3. Director solution $\theta(z)$ for different values of the material parameter Υ while keeping $D = 10$. $\Upsilon = 0$ corresponds to a NLC layer with no flexoelectric contribution. $\Upsilon = 1$ corresponds to the director configuration shown in Fig. 2(b).

IV. STABILITY ANALYSIS AND BIFURCATIONS FOR SYMMETRIC ANCHORING CONDITIONS

We now investigate how changing the flexoelectric strength affects the Fredericksz and saturation thresholds in a nematic liquid crystal layer (these thresholds have been extensively studied in the absence of flexoelectricity, see, e.g., [2,8,9,14,25]). In order to do this, we first identify certain properties of Eqs. (8) as well as introduce measures that allow us to quantify our findings. We observe that, with $\alpha_0 = \alpha_1 = \pi/2$, in addition to nontrivial director solutions of the type seen in Figs. 2 and 3 (which we now call θ_n), the boundary value problem [Eqs. (8)] admits two additional steady-state solutions that exist for all values of D , \mathcal{F} : $\theta_v(z,t) = 0$ (a vertical state) and $\theta_h(z,t) = \pi/2$ (a horizontal state). These solutions are linearly stable only if, when subjected to sufficiently small perturbations, such perturbations die away and the steady state is recovered at large times. Linear stability of each solution type depends on the choice of model parameters, and can be determined either numerically or analytically (see Appendix for details of our analytical approach). Solutions gain or lose stability as model parameters are varied, and this may be visualized by constructing bifurcation diagrams. In order to construct such diagrams, we plot the norm $\|\dots\|_2$, of the steady-state director solution, defined as

$$\|\theta\|_2 = \sqrt{\int_0^1 \theta^2 dz}.$$

Since the three distinct solutions θ_h , θ_n , θ_v have different norms, bifurcations between solution types are clearly visible. Figure 4 illustrates the bifurcation diagram obtained by plotting $\|\theta\|_2$ as a function of \mathcal{F} for several different values of the material parameter Υ , which characterizes the strength of the flexoelectric effect. The diagram is obtained using the continuation method as follows: since we anticipate that the horizontal state is a unique steady solution at zero field, we use a weakly perturbed state $\theta = \pi/2 - \delta$ as the initial condition when $\mathcal{F} = 0$. We then slowly increase \mathcal{F} from $\mathcal{F} = 0$, always

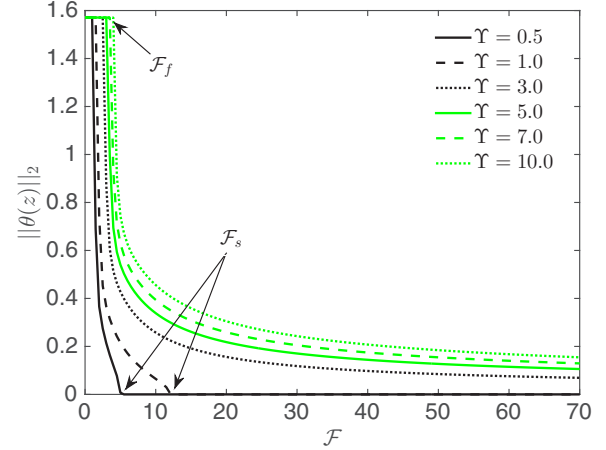


FIG. 4. Bifurcation diagram showing $\|\theta(z)\|_2$ vs \mathcal{F} with $\mathcal{A}_0 = \mathcal{A}_1 = 5$ and $\alpha_0 = \alpha_1 = \pi/2$ for different Υ , obtained using continuation in \mathcal{F} . \mathcal{F}_f denotes the Fredericksz threshold and \mathcal{F}_s denotes the saturation threshold with the arrows pointing where the thresholds occur for each Υ .

using the solution obtained with the previously used smaller value of \mathcal{F} (forward continuation). We also carry out reverse continuation using a similar process: since we anticipate that the vertical state is a unique steady solution at electric field strengths above the saturation threshold ($\mathcal{F} > \mathcal{F}_s$), we use this state with a small perturbation, $\theta = \delta$, as the initial condition for the largest value of \mathcal{F} , and thereafter decrease \mathcal{F} , at each stage using the previous large-time solution as the new initial condition. When generating our bifurcation diagrams (Figs. 4–10), both forward and reverse continuations are carried out to reveal any bistability that might be present for a range of electric field strengths. In Figs. 4 and 5, however, we

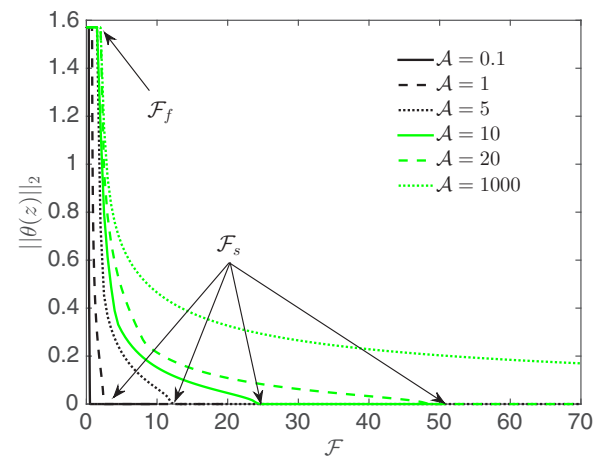


FIG. 5. Bifurcation diagram showing $\|\theta(z)\|_2$ vs \mathcal{F} with $\Upsilon = 1$ for different anchoring strengths: $\mathcal{A}_0 = \mathcal{A}_1 = 0.1, 1, 5, 10, 20, 1000$ obtained using continuation in \mathcal{F} . The portion of the diagram where $\|\theta\|_2 = \pi/2$ represents the horizontal state $[\theta_h(z) = \pi/2]$, while $\|\theta\|_2 = 0$ represents the vertical state $[\theta_v(z) = 0]$. The intermediate portion (slowly decaying as $|\mathcal{F}|$ increases) represents the nontrivial solution $\theta_n(z)$ found numerically.

show results for $\mathcal{F} \geq 0$ only {since changing the electric field direction $\mathcal{F} \rightarrow -\mathcal{F}$ simply flips the director solution profile θ about the centerline $z = 0.5$ [see Figs. 2(b) and 2(c)] leading to bifurcation diagrams symmetric about the vertical axis}, and for forward continuation only (since the system is found to be monostable).

For the range of \mathcal{F} values considered here, Fig. 4 shows that, for small values of Υ (specifically $\Upsilon = 0.5$ and 1), three director configurations are found: the horizontal ($\|\theta_h\|_2 = \pi/2$) represented by the upper left portion of the graph for all Υ , the nontrivial ($0 < \|\theta_n\|_2 < \pi/2$) and the vertical ($\|\theta_v\|_2 = 0$) solutions. In these two cases, the director configuration transitions as follows: at low \mathcal{F} values the horizontal solution θ_h is obtained. Then, if \mathcal{F} passes a critical value \mathcal{F}_f (Freedericksz transition), the nontrivial solution θ_n is observed. As \mathcal{F} is increased further still, past a second critical value \mathcal{F}_s (saturation threshold), the vertical solution θ_v is observed.

These observations are as expected, but the question of how flexoelectricity affects these results has not yet been addressed. Looking at Fig. 4, we observe that both threshold values increase with Υ . While the Freedericksz threshold \mathcal{F}_f is present for all values of Υ considered, the saturation threshold is only seen for the lowest two values of Υ , at least for the range of \mathcal{F} values considered here. In order to determine whether the saturation threshold is present for all $\Upsilon \geq 0$, we use an analytical approach based on the calculus of variations. We study specifically the stability of the vertical solution $\theta_v = 0$. If it can be shown that θ_v is always stable for sufficiently large \mathcal{F} , then we may conclude that a saturation threshold \mathcal{F}_s should exist, for all $\Upsilon \geq 0$.

The calculus of variations approach proceeds by directly seeking minimizers $\theta(z)$ of the total free energy $J = h^* J^*/K^*$ [where J^* is defined in Eq. (4)]. Small perturbations to a minimizer, $\theta(z) \rightarrow \theta(z) + \epsilon\eta(z)$, ($0 < \epsilon \ll 1$) induce variations in J : $J \rightarrow J[\theta + \epsilon\eta] = J_0 + \epsilon J_1 + \epsilon^2 J_2 + \mathcal{O}(\epsilon^3)$. For $\theta(z)$ to be a free energy minimizer, we require $J_1 = 0$ and $J_2 > 0$ for all admissible variations η (see Appendix for more details). Upon obtaining expressions for J_1 and J_2 [see Eqs. (A6)–(A8) in Appendix], it may be seen that, for $\theta(z) = \theta_v = 0$ and any $\Upsilon > 0$, we have $J_1 = 0$, and for sufficiently large $|\mathcal{F}|$ the second variation $J_2 > 0$, hence, $\theta(z) = 0$ is a stable solution for such \mathcal{F} . It may also be seen from Eq. (A8) that the larger the value of Υ , the larger \mathcal{F} must be to guarantee positivity of J_2 for all admissible variations η . Similarly, we are able to show that the horizontal solution $\theta(z) = \theta_h = \pi/2$ is stable for sufficiently small $|\mathcal{F}|$. Hence, the calculus of variations allows us to conclude that inclusion of flexoelectric effects in the model does not affect the fundamental mathematical structure of the system: with the weak anchoring considered here, both Freedericksz and saturation thresholds (\mathcal{F}_f and \mathcal{F}_s) always exist, both being increasing functions of Υ . We note, for completeness, that the $\Upsilon = 10$ result in Fig. 4 may lie in the regime where the uniform field approximation begins to lose validity [13].

We next investigate how the strength of the surface anchoring (here assumed the same at both boundaries) affects results, for a fixed value of the material parameter Υ . We consider a range of anchoring strength values from $\mathcal{A}_0 = \mathcal{A}_1 = 0.1$ to $\mathcal{A}_0 = \mathcal{A}_1 = 1000$ and obtain a bifurcation diagram by plotting

$\|\theta\|_2$ as a function of \mathcal{F} . As shown in Fig. 5, we observe that both Freedericksz and saturation thresholds are present for all except the largest value of \mathcal{A} used, and both thresholds increase with \mathcal{A} . As before, where our numerics are inconclusive, we may augment with an analytical approach. The calculus of variations technique outlined earlier again reveals that the vertical solution θ_v is stable for sufficiently large \mathcal{F} and finite \mathcal{A} . Note that in the limit as $\mathcal{A} \rightarrow \infty$, positivity of the second variation $J_2 > 0$ [see Eq. (A8) in the Appendix] is not guaranteed, as we recover the Freedericksz transition cell with strong anchoring where the saturation threshold and therefore the vertical solution disappear.

Figures 4 and 5 verify the prediction of [7] that there exists a polarity independent flexoelectrically enhanced Freedericksz transition. Indeed, we find that the Freedericksz threshold value is independent of the direction of the electric field. In addition, we observe that the saturation threshold increases with $|\mathcal{F}|$ and it is also independent of the direction of the electric field. We remind the reader that for the cases considered in Figs. 4 and 5, the system is monostable: only one steady director configuration is stable for a given electric field strength. In the following section, we consider how breaking the symmetry in the anchoring conditions, specifically, changing the anchoring strength and anchoring angles at each boundary, affects the mathematical structure of the system.

V. STABILITY ANALYSIS AND BIFURCATIONS FOR ASYMMETRIC ANCHORING CONDITIONS

The coexistence of two (or more) *stable* director configurations gives rise to the potential for development of bistable LCD devices, noted in the Introduction. If two stable states exist at zero field, then contrast between neighboring pixels could be maintained without use of energy, with an electric field needed only to switch pixels from one configuration to the other as needed [10, 11, 23, 24, 28, 29]. In our model represented by Eqs. (8) we find that breaking the symmetry of the anchoring conditions can lead to bistability. In the following section, we see how such bistability arises, and study the effect of flexoelectricity on director profiles, with particular attention paid to how the Freedericksz and saturation threshold are affected.

A. Asymmetric anchoring strengths

We begin our investigation into anchoring asymmetry by maintaining planar anchoring at both boundaries ($\alpha_0 = \alpha_1 = \pi/2$), but allowing anchoring strengths to differ. We keep the lower anchoring strength constant at $\mathcal{A}_0 = 10$ and vary the upper anchoring strength in the range $1 \leq \mathcal{A}_1 \leq 12$. We expect the system to retain the same qualitative features of a weak Freedericksz transition cell where all three director configurations (θ_h , θ_n , and θ_v) seen in Fig. 5 persist despite the different anchoring strengths at each boundary. However, due to the loss of symmetry in the anchoring strength and the inherent dependence of the flexoelectric effect on the direction of the electric field (see [7]), we now anticipate results for $\mathcal{F} < 0$ to differ from those for $\mathcal{F} > 0$.

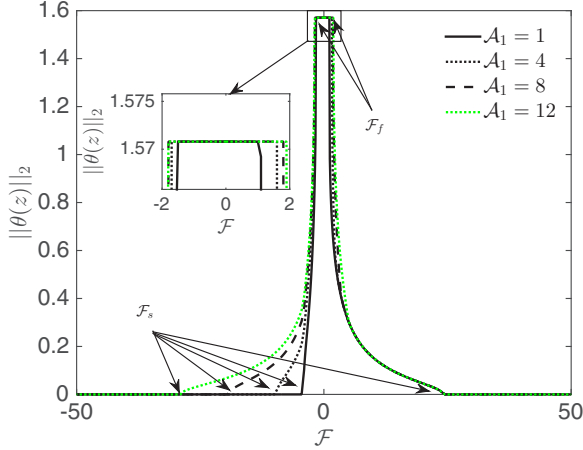


FIG. 6. Bifurcation diagram showing $\|\theta(z)\|_2$ vs \mathcal{F} with $\Upsilon = 1$ for $\mathcal{A}_0 = 10.0$ and $1 \leq \mathcal{A}_1 \leq 12$ using continuation in \mathcal{F} .

Figure 6 illustrates the bifurcation diagram, obtained by forward continuation in $|\mathcal{F}|$ from $\mathcal{F} = 0$, showing the stable director configurations for a range of values of \mathcal{A}_1 . Here, as in Figs. 4 and 5, we use a slightly perturbed horizontal state as an initial condition when $\mathcal{F} = 0$, followed by the solution obtained with the previous electric field strength when $\mathcal{F} \neq 0$ (continuation). For this particular set of simulations, the size of the Fredericksz threshold, $|\mathcal{F}_f|$, increases with \mathcal{A}_1 (see inset of Fig. 6). We also observe that the Fredericksz threshold at positive \mathcal{F} , \mathcal{F}_f^+ is different than the Fredericksz threshold at negative \mathcal{F} , $|\mathcal{F}_f^-|$ for each anchoring strength considered. This observation confirms and quantifies the predictions of Derzhanski *et al.*, who stated that if the anchoring strength is different at each boundary, $\mathcal{A}_0 \neq \mathcal{A}_1$, there exists a polarity dependent flexoelectrically enhanced Fredericksz transition.

Figure 6 also shows that the saturation threshold at positive \mathcal{F} , (\mathcal{F}_s^+) appears to be essentially independent of \mathcal{A}_1 ; but, its value at negative \mathcal{F} , (\mathcal{F}_s^-) depends strongly on \mathcal{A}_1 , with $|\mathcal{F}_s^-|$ being an increasing function of \mathcal{A}_1 . The dependence of the saturation threshold for positive and negative values of \mathcal{F} (denoted by $\mathcal{F}_s^{(+,-)}$) on $\mathcal{A}_{[0,1]}$ can be understood by considering the behavior of the nontrivial director solution θ_n with weak anchoring (recall that this solution exists only for \mathcal{F} values between the Fredericksz and saturation thresholds; see, e.g., Fig. 2 for the symmetric weak anchoring case). Consider the case $\mathcal{F} > 0$ first. It is clear from Fig. 2(b) that, where θ_n exists, the director behavior is very different at the two boundaries, respecting the anchoring at $z = 0$ but aligning with the field at $z = 1$. Since the director is already field aligned at $z = 1$, we would not anticipate that the anchoring strength at that boundary will have much effect on the saturation threshold value at which the director solution switches to the fully aligned state; the value of \mathcal{A}_0 will be more important. When $\mathcal{F} < 0$, however, the situation is reversed: the director is field aligned at $z = 0$, while strongly influenced by the surface anchoring at $z = 1$ [Fig. 2(c)]. In this case, we expect the value of \mathcal{A}_1 to have a significant effect on the saturation threshold, and this is borne out in Fig. 6.

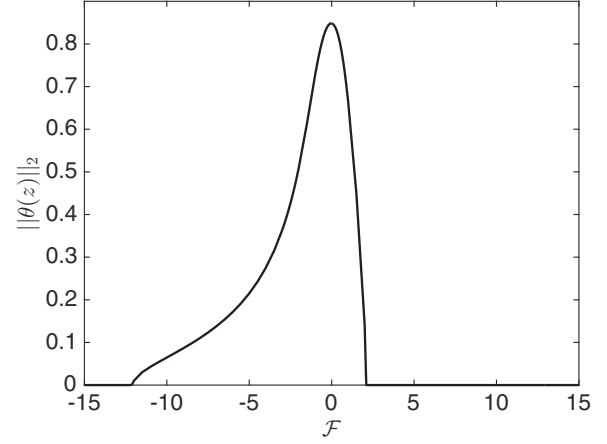


FIG. 7. Bifurcation diagram showing $\|\theta(z)\|_2$ vs \mathcal{F} with $\Upsilon = 1$ for $\mathcal{A}_0 = \mathcal{A}_1 = 5$ and $\alpha_0 = 0$, $\alpha_1 = \pi/2$, obtained using continuation in \mathcal{F} .

B. Asymmetric anchoring angles

We next investigate how perturbations in the anchoring angles can change the structure of the system, in particular, how the Fredericksz and saturation thresholds are affected. We begin by considering a system that is somewhat special: anchoring angles $\alpha_0 = 0$ and $\alpha_1 = \pi/2$; this is commonly referred to as the hybrid aligned state, which we here call the semisymmetric system. The anchoring strengths are set to $\mathcal{A}_0 = \mathcal{A}_1 = 5$ throughout the section. Inspection of Eqs. (8) reveals that in this case the horizontal and vertical solutions $\theta_h = \pi/2$ and $\theta_v = 0$ are still steady solutions, but now we anticipate that θ_h may no longer be stable at small nonzero fields since it is favored by just one (not both) boundaries. Hence, we expect to see only a saturation threshold as $|\mathcal{F}|$ is increased from zero.

Figure 7 shows the bifurcation diagram for this case. In obtaining the director solutions for each \mathcal{F} , we first use $\theta = \pi/2 - \delta$ as an initial guess when $\mathcal{F} = 0$, and thereafter use forward continuation in $|\mathcal{F}|$ (reverse continuation was also carried out with identical results obtained; the system is monostable). We observe that, as anticipated, the horizontal state is never stable. Instead, the system converges to a nontrivial state θ_n , which is stable for small values of $|\mathcal{F}|$. For large enough $|\mathcal{F}|$, the vertical state $\theta_v(z) = 0$ becomes stable while the nontrivial steady state is unstable (or ceases to exist). This asymmetry in the saturation threshold is due to the flexoelectricity. We conclude that this system does not have a Fredericksz threshold, only a saturation threshold, which occurs at $\mathcal{F} \approx -12.5$ for $\mathcal{F} < 0$ and $\mathcal{F} \approx 2.5$ for $\mathcal{F} > 0$.

For $\mathcal{F} > 0$, flexoelectricity helps the director fully align with the electric field at weaker field strength than for $\mathcal{F} < 0$. This can be explained in terms of the nontrivial director configuration for asymmetric anchoring conditions $\alpha_0 = 0$ and $\alpha_1 = \pi/2$. In the absence of an electric field, the director configuration is linear in z , satisfying the anchoring conditions (8b) and (8c) at the boundaries. As an electric field is applied in the positive z direction, the molecules in the bulk and at the upper boundary align with the electric field [cf. Fig. 2(b)]. Here, however, the molecules at the lower boundary

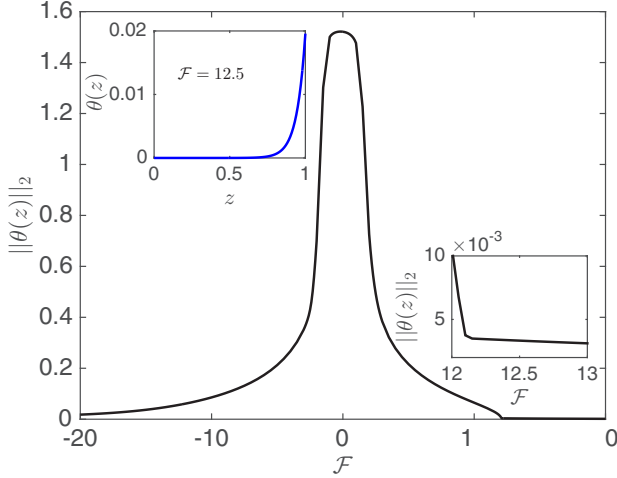


FIG. 8. Bifurcation diagram showing $\|\theta(z)\|_2$ vs \mathcal{F} with $\Upsilon = 1$ for $\mathcal{A}_0 = \mathcal{A}_1 = 5$ and $\alpha_0 = \pi/2, \alpha_1 = \pi/2 - \psi$ ($\psi = 0.1$), obtained using forward continuation in \mathcal{F} . Inset located at the upper left corner shows the director configuration obtained when $\mathcal{F} = 12.5$. Inset located at the lower right corner shows a zoom of the bifurcation diagram, to clarify the behavior in the range $12 \leq \mathcal{F} \leq 13$ region.

are already aligned with the applied field, hence, a fairly low field strength suffices to make the transition from nontrivial to vertical state. On the other hand, when $\mathcal{F} < 0$, the molecules at the upper boundary are dominated by the planar anchoring [cf. Fig. 2(c)], and in this case, a much higher field is needed to effect the transition from nontrivial to vertical state.

With a clear picture of the system behavior for the two special cases of (i) equal strength planar anchoring at both boundaries ($\alpha_0 = \alpha_1 = \pi/2$, symmetric case) and (ii) equal strength anchoring that is homeotropic at one boundary and planar at the other ($\alpha_0 = 0, \alpha_1 = \pi/2$, semisymmetric case), we now investigate how small perturbations to such anchoring conditions change system behavior. We maintain the anchoring strengths $\mathcal{A}_0 = \mathcal{A}_1 = 5$ at each boundary and introduce a small perturbation ψ to the anchoring angles as follows: (i) $\alpha_0 = \pi/2, \alpha_1 = \pi/2 - \psi$, (ii) $\alpha_0 = 0, \alpha_1 = \pi/2 - \psi$, and (iii) $\alpha_0 = \psi, \alpha_1 = \pi/2$. We set $\psi = 0.1$ in all simulations that follow.

Figure 8 shows the bifurcation diagram where $\|\theta(z)\|_2$ is plotted as a function of \mathcal{F} for $\alpha_0 = \pi/2$ and $\alpha_1 = \pi/2 - \psi$. As in the previous cases, we first use a slightly perturbed horizontal state $\theta = \pi/2 - \delta$ as initial condition when $\mathcal{F} = 0$, and thereafter use forward continuation in $|\mathcal{F}|$. Since the system is monostable, reverse continuation starting from $|\mathcal{F}| = 20$ with initial condition $\theta = \delta$ leads to identical results. We note that θ_h and θ_v are no longer steady-state solutions that satisfy Eqs. (8) for the given anchoring angles, hence, we do not expect to observe true Fredericksz and saturation thresholds. At zero electric field strength, a nontrivial director solution (nearly horizontal) satisfies the anchoring angles with $\|\theta(z)\|_2 = 1.52$. As $|\mathcal{F}|$ increases, the nontrivial solution evolves, becoming rapidly more vertical. Observe that, for $\mathcal{F} \approx 12$, it appears that a saturation threshold is reached, however, closer examination (the inset located at the lower right corner in Fig. 8) reveals that in fact the director never fully breaks the surface anchoring to reach the strictly vertical state

$\theta_v = 0$. A boundary layer near $z = 1$ persists (see inset located at the upper left corner of Fig. 8). Note that the bifurcation diagram shown in Fig. 8 is far from symmetric in \mathcal{F} , being significantly altered from its equivalent (shown in Figs. 4 and 5, reflected about the vertical axis) when $\psi = 0$. This asymmetry is induced purely by the flexoelectric effect. In the absence of flexoelectricity, $\Upsilon = 0$, the bifurcation diagram is symmetric in \mathcal{F} .

We now consider perturbations to the system with homeotropic anchoring at one boundary and planar anchoring at the other, with (ii) $\alpha_0 = \psi, \alpha_1 = \pi/2$ and (iii) $\alpha_0 = 0, \alpha_1 = \pi/2 - \psi$. Once more, θ_h and θ_v are no longer steady-state solutions that satisfy Eqs. (8) for the given anchoring angles. Hence, we do not expect to observe the Fredericksz or saturation thresholds. In fact, both cases (ii) and (iii) are bistable [10,11], admitting two nontrivial director configurations $\theta_{n,1}$ and $\theta_{n,2}$, hence, we must track both solutions in our bifurcation diagrams.

Figure 9 shows the bifurcation diagrams for cases (ii) and (iii), where $\|\theta(z)\|_2$ is plotted as a function of \mathcal{F} for each solution. Since two director configurations exist in the absence of an electric field, we obtain two director solutions for each \mathcal{F} by using $\theta_{n,1}$ and $\theta_{n,2}$ as initial conditions, followed by forward continuation in $|\mathcal{F}|$. In addition, we use a perturbed vertical state $\theta(z) = \delta$ as the initial condition for large $|\mathcal{F}|$ followed by reverse continuation.

Figure 9(a) shows the bifurcation diagram for $\alpha_0 = \psi$ and $\alpha_1 = \pi/2$. We observe that when $|\mathcal{F}|$ is small, two stable director configurations given by $\theta_{n,1}$ and $\theta_{n,2}$ exist (solid black line showing the norm of $\theta_{n,1}$ and red dashed line showing the norm of $\theta_{n,2}$). As $|\mathcal{F}|$ increases, one of the solutions disappears; both director solutions have the same norm. Reverse continuation (green dots) converges to the director configuration given by $\theta_{n,1}$ which means that one can switch from $\theta_{n,2} \rightarrow \theta_{n,1}$ by increasing $|\mathcal{F}|$ but not vice versa. This poses an inconvenience from an applications point of view since, to be useful, a bistable system must allow two-way switching (see [10,11] for a more detailed investigation of bistability and switching).

As already noted, since θ_h and θ_v are not solutions to this perturbed system, there can be no true Fredericksz or saturation threshold. Similarly to Fig. 8, Fig. 9(a) has an apparent bifurcation (at $\mathcal{F} \approx -12.5$) but again the inset reveals that the solution is never fully vertical.

Figure 9(b) shows the bifurcation diagram for $\alpha_0 = 0$ and $\alpha_1 = \pi/2 - \psi$. As above, we observe that two director configurations $\theta_{n,1}$ and $\theta_{n,2}$ exist for small values of $|\mathcal{F}|$, indicating that the system is bistable. As $|\mathcal{F}|$ increases, the system loses its bistability. Note that for $\mathcal{F} \approx -5$ the two solutions have the same norm in Fig. 9(b): this does not, however, imply that the director configurations are identical. In fact when $\mathcal{F} \approx -5$, $\theta_{n,1}$ and $\theta_{n,2}$ are distinct solutions, which just happen to have the same $\|\theta(z)\|_2$ norm, so the system is still bistable here. As \mathcal{F} increases further, however, the system can no longer sustain two stable steady states. Figure 9(b) shows that the system loses bistability at $\mathcal{F} \approx -7.4$ for $\mathcal{F} < 0$ and $\mathcal{F} \approx 2$ for $\mathcal{F} > 0$. Beyond these two values the system is monostable. It is curious to note how different the bifurcation structures in Figs. 9(a) and 9(b) are, in particular at negative \mathcal{F} values, while the underlying models are so close.

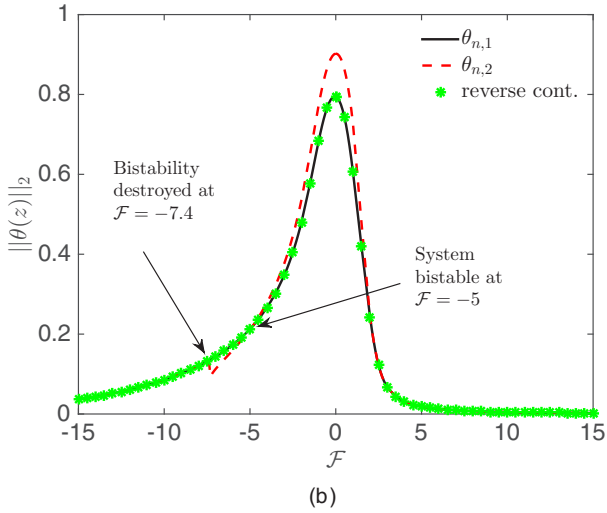
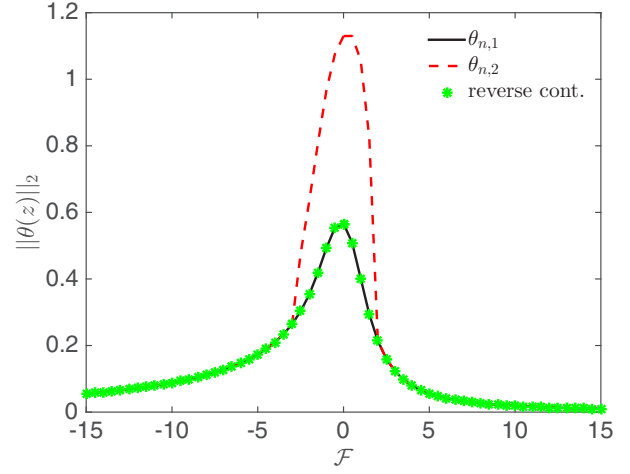
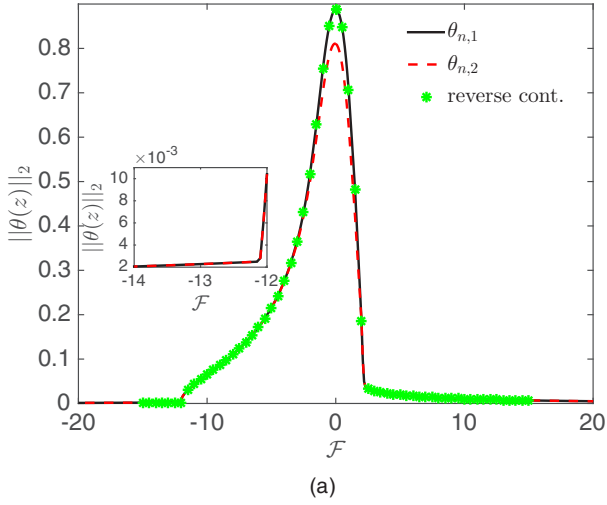


FIG. 9. Bifurcation diagram showing $\|\theta(z)\|_2$ plotted vs \mathcal{F} with $\Upsilon = 1$ for (a) $\alpha_0 = \psi$ and $\alpha_1 = \pi/2$ and (b) $\alpha_0 = 0$, $\alpha_1 = \pi/2 - \psi$ (with $\psi = 0.1$). Anchoring strengths are set to $\mathcal{A}_0 = \mathcal{A}_1 = 5$. Black solid and red dashed curves are obtained using forward continuation in $|\mathcal{F}|$ while the green dotted curve is obtained using reverse continuation in $|\mathcal{F}|$.

Finally, we present an example with fully asymmetric boundary conditions $\alpha_0 = 0$ and $\alpha_1 = \pi/3$. Here, as in Figs. 4–9, we plot $\|\theta(z)\|_2$ as a function of \mathcal{F} by using forward and reverse continuation methods. The behavior of the system is similar to the perturbed semisymmetric cases shown in Fig. 9: the system is initially bistable with two director configurations $\theta_{n,1}$ and $\theta_{n,2}$ and loses bistability as $|\mathcal{F}|$ increases. Also, θ_h and θ_v again do not exist, hence, there are no Freedericksz and saturation thresholds. As in Fig. 9, we observe that one can switch only from $\theta_{n,2} \rightarrow \theta_{n,1}$ by increasing $|\mathcal{F}|$. Since reverse continuation favors $\theta_{n,1}$, we cannot switch from $\theta_{n,1} \rightarrow \theta_{n,2}$ in the asymmetric cases shown here. This finding exemplifies some of the difficulties inherent in designing bistable devices.

Figures 6–10 have shown that changing the anchoring conditions, even slightly, significantly alters the director configurations present in a Freedericksz transition cell as well as its bifurcation properties (the Freedericksz and saturation

FIG. 10. Bifurcation diagram showing $\|\theta(z)\|_2$ plotted vs \mathcal{F} with $\Upsilon = 1$ for $\alpha_0 = 0$ and $\alpha_1 = \pi/3$. Anchoring strengths are set to $\mathcal{A}_0 = \mathcal{A}_1 = 5$. Black solid and red dashed curves are obtained using forward continuation in $|\mathcal{F}|$ while the green dotted curve is obtained using reverse continuation in $|\mathcal{F}|$.

thresholds). In particular, we observe that changing the anchoring strength \mathcal{A} simply increases the Freedericksz and saturation threshold values. Breaking the symmetry in the anchoring angles, however, changes the structure of the cell, eliminating the purely horizontal and vertical states present in a classic Freedericksz transition cell. In doing so, one can eliminate both Freedericksz and saturation thresholds.

VI. CONCLUSIONS

We have presented a mathematical model that describes the evolution of the director field within a confined layer of nematic liquid crystal where an electric field is applied in the z direction and the anchoring conditions vary. We investigate in detail how an applied electric field affects the evolution of the director field in the presence of both dielectric and flexoelectric effects for strong and weak anchoring. We observe that for strong planar anchoring the director aligns vertically in the direction of the electric field in the interior of the layer and aligns nearly parallel to the anchoring angles close to the interface; flexoelectric effects are not observed. In the case of weak planar anchoring, flexoelectricity significantly affects the system's behavior. We find that, at intermediate values of the electric field strength, the director aligns parallel to the electric field in the interior of the layer and at one of the boundaries (which boundary depends on the direction of the electric field). The key characteristics of a weak Freedericksz transition cell persist, however: three director solutions (which we call θ_h , θ_n , and θ_v for horizontal, nontrivial, and vertical states) exist, only one of which is stable at a given electric field strength. Solution θ_h is stable for $0 < \mathcal{F} < \mathcal{F}_f$ (the Freedericksz transition threshold); solution θ_n is stable for $\mathcal{F}_f < \mathcal{F} < \mathcal{F}_s$ (the saturation threshold) and solution θ_v is stable for $\mathcal{F} > \mathcal{F}_s$.

We pay particular attention to the above transition structure when increasing the effect of flexoelectricity by varying the material parameter $\Upsilon = \mathcal{F}^2/D$ [see Eq. (10)]. We observe

that both Fredericksz and saturation thresholds increase with flexoelectricity. In addition, we investigate how the Fredericksz and saturation thresholds change as anchoring conditions are varied at each boundary. When the anchoring strength parameters ($\mathcal{A}_{\{0,1\}}$) are varied, we observe that the stability of the director configurations does not change, but the Fredericksz and saturation thresholds increase with \mathcal{A} . When investigating a system with planar anchoring angles ($\alpha_0 = \alpha_1 = \pi/2$) while varying the anchoring strength only at one boundary, we observe that the structure of the system and the saturation threshold at positive \mathcal{F} , \mathcal{F}_s^+ , remain unchanged (three director configurations exist: θ_h , θ_n , and θ_v). The Fredericksz threshold for both positive and negative \mathcal{F} , $\mathcal{F}_f^{(+,-)}$, and the saturation threshold for negative \mathcal{F} , \mathcal{F}_s^- , increase in magnitude with \mathcal{A}_1 . Finally, changing the anchoring angles at the boundaries (nonplanar anchoring angles) reveals that the structure and stability of the possible director configurations change fundamentally. Here, the horizontal and vertical states are no longer solutions. In some cases bistability is observed, with more than one nontrivial director solution. We find that, while bistability is preserved for weak applied fields, it is typically lost for stronger fields. As the applied field is increased, the system tends to become monostable.

Finally, in the Appendix, we present two analytical approaches that help us determine the stability of the director configurations for the weak Fredericksz transition cells. We use the calculus of variations to minimize the total free energy of the system and determine the stability of the horizontal and vertical director configurations. We also carry out linear stability analysis by linearizing Eqs. (8) around the purely vertical and horizontal solutions and we determine whether perturbations to these solutions exhibit growth or decay in time. We find that our numerical results are strongly supported by the analytical ones.

ACKNOWLEDGMENT

This work was supported by the NSF under Grant No. DMS-1211713.

APPENDIX

We augment our numerical approach in the main paper by two analytical approaches to determine the stability of the steady solutions to Eq. (8). The first consists of using the calculus of variations to calculate the first and second variation of the total free energy of the system. In certain cases, we can show that the second variation of a particular solution θ (a zero of the first variation) is either strictly positive (energy minimum; stable) or strictly negative (energy maximum; unstable).

We also use linear stability analysis (LSA) as our second approach where we linearize Eqs. (8) around the two solutions that are known explicitly [$\theta_v(z, t) = 0$, $\theta_h(z, t) = \pi/2$] and seek to determine whether perturbations to these solutions exhibit growth or decay in time.

1. Calculus of variations

We determine the stability of the steady solutions $\theta_i(z) = 0$ and $\theta_h(z) = \pi/2$ in the presence of an external field. Since

we will consider only the equilibrium solutions, we omit the t dependence. The total free energy for our system is given by

$$J = \int_0^1 W(\theta, \theta_z) dz + g_0(\theta)|_{z=0} + g_1(\theta)|_{z=1}, \quad (\text{A1})$$

where W , g_0 , and g_1 are the dimensionless bulk and surface energy densities obtained by nondimensionalizing Eq. (4) using the scales in Eqs. (7):

$$W = \frac{\theta_z^2}{2} - \mathcal{D} \cos^2 \theta + \frac{\mathcal{F} \theta_z}{2} \sin 2\theta, \quad (\text{A2})$$

$$g_{\{0,1\}} = \frac{\mathcal{A}_{\{0,1\}}}{2} \sin^2(\theta - \alpha_{\{0,1\}}). \quad (\text{A3})$$

We look for equilibrium solutions $\theta(z)$ that minimize J as follows: let $\theta(z) \rightarrow \theta(z) + \epsilon \eta(z)$ ($0 < \epsilon \ll 1$): this assumption leads to $J \rightarrow J[\theta + \epsilon \eta] = J_0 + \epsilon J_1 + \epsilon^2 J_2 + \mathcal{O}(\epsilon^3)$. For $\theta(z)$ to be a minimizer of J (a stable solution), we require $J_1 = 0$ and $J_2 > 0$ for all admissible variations η . If on the other hand $J_2 < 0$, then we have a local maximum of the free energy, and hence an unstable steady solution. After Taylor expansion, the expression for J_1 takes the following form:

$$J_1 = \int_0^1 \eta [W_\theta - (W_{\theta_z})_z] dz + \eta (g_{1\theta} + W_{\theta_z})|_{z=1} + \eta (g_{0\theta} - W_{\theta_z})|_{z=0}. \quad (\text{A4})$$

After integration by parts, the second variation J_2 can be expressed as follows:

$$J_2 = \frac{1}{2} \int_0^1 \{ \eta^2 [W_{\theta\theta} - (W_{\theta\theta_z})_z] + \eta_z^2 W_{\theta_z\theta_z} \} dz + \eta^2 (g_{1\theta\theta} + W_{\theta\theta_z})|_{z=1} + \eta^2 (g_{0\theta\theta} - W_{\theta\theta_z})|_{z=0}. \quad (\text{A5})$$

We check the stability of the director solution $\theta_v(z) = 0$ and $\theta_h(z) = \pi/2$ by evaluating J_2 when $\alpha_{\{0,1\}} = \pi/2$ (J_1 must always vanish for any steady solution).

a. Stability of director solution $\theta_v(z) = 0$

Substituting W and $g_{\{0,1\}}$ given by Eqs. (A2) and (A3) into J_1 and J_2 [see Eqs. (A4) and (A5)] and manipulating the expressions, we first verify that $J_1 = 0$ for $\theta(z) = 0$, and that $J_2 > 0$ for sufficiently large \mathcal{F} . The first and second variations are evaluated as

$$J_1 = \int_0^1 \eta [\mathcal{D} \sin 2\theta - \theta_{zz}] dz + \eta \left[\frac{\mathcal{A}_1}{2} \sin 2(\theta - \alpha_1) + \theta_z + \frac{\mathcal{F}}{2} \sin 2\theta \right] \Big|_{z=1} + \eta \left[\frac{\mathcal{A}_0}{2} \sin 2(\theta - \alpha_0) - \theta_z - \frac{\mathcal{F}}{2} \sin 2\theta \right] \Big|_{z=0}, \quad (\text{A6})$$

$$J_2 = \frac{1}{2} \int_0^1 \eta^2 [2\mathcal{D} \cos 2\theta - 2\mathcal{F} \theta_z \sin 2\theta - 2\mathcal{F} \theta_z \cos 2\theta] dz + \frac{1}{2} \int_0^1 \eta_z^2 dz + \eta^2 [\mathcal{A}_1 \cos 2(\theta - \alpha_1) + \mathcal{F} \cos 2\theta] \Big|_{z=1} + \eta^2 [\mathcal{A}_0 \cos 2(\theta - \alpha_0) - \mathcal{F} \cos 2\theta] \Big|_{z=0}. \quad (\text{A7})$$

We assume that the two surface energies are equal, $\mathcal{A}_0 = \mathcal{A}_1$. Setting $\theta = \theta_v = 0$, $J_1 = 0$ and J_2 simplifies to

$$J_2 = \frac{1}{2} \int_0^1 \left\{ 2 \frac{\mathcal{F}^2}{\Upsilon} \eta^2 + \eta_z^2 \right\} dz - \frac{\mathcal{A}}{2} (\eta^2|_{z=1} + \eta^2|_{z=0}) + \frac{\mathcal{F}}{2} (\eta^2|_{z=1} - \eta^2|_{z=0}). \quad (\text{A8})$$

Observe that the first term in Eq. (A8) dominates for larger $|\mathcal{F}|$ and we conclude the following: when $|\mathcal{F}|$ is sufficiently large and for finite anchoring strength \mathcal{A} and finite values of Υ , $J_2 > 0$. This establishes that $\theta(z) = 0$ is a minimum energy solution and therefore stable.

Similarly, we can determine the sign of J_2 in the limiting case when $\mathcal{F} \rightarrow 0$ and anchoring is sufficiently strong. We obtain

$$J_2 \approx \frac{1}{2} \int_0^1 \eta_z^2 dz + \eta^2(-\mathcal{A} + \mathcal{F})|_{z=1} + \eta^2(-\mathcal{A} - \mathcal{F})|_{z=0}$$

for $|\mathcal{F}| \ll \mathcal{A}$, which leads to the following result: when $|\mathcal{F}|$ is sufficiently small and simultaneously \mathcal{A} is sufficiently large, $J_2 < 0$ and $\theta(z) = 0$ is a solution locally maximizing the free energy and therefore unstable.

b. Stability of director solution $\theta_h(z) = \pi/2$

A similar approach is taken to determine the stability of $\theta_h(z) = \pi/2$ for large $|\mathcal{F}|$. We first check that $J_1 = 0$ for $\theta_h(z) = \pi/2$, which a glance at Eq. (A6) confirms. Calculating the second variation J_2 for $\theta_h(z) = \pi/2$ by letting $\mathcal{D} = \mathcal{F}^2/\Upsilon$ and $\mathcal{A}_0 = \mathcal{A}_1$ in Eq. (A7), we obtain

$$J_2 = \frac{1}{2} \left[\int_0^1 -2 \frac{\mathcal{F}^2}{\Upsilon} \eta^2 dz + \int_0^1 \eta_z^2 dz + \eta^2(\mathcal{A} - \mathcal{F})|_{z=1} + \eta^2(\mathcal{A} + \mathcal{F})|_{z=0} \right]. \quad (\text{A9})$$

As before, we conclude that when $|\mathcal{F}|$ is sufficiently large and \mathcal{A} is finite, $J_2 < 0$, establishing that $\theta_h(z) = \pi/2$ is a local energy maximizer and therefore unstable.

Similarly, we can determine the sign of J_2 for $\theta(z) = \pi/2$ in the limiting case when $\mathcal{F} \rightarrow 0$. We obtain from Eq. (A9)

$$J_2 \approx \int_0^1 \eta_z^2 dz + \eta^2(\mathcal{A} - \mathcal{F})|_{z=1} + \eta^2(\mathcal{A} + \mathcal{F})|_{z=0}$$

and we conclude that when $|\mathcal{F}|$ is sufficiently small and simultaneously \mathcal{A} is sufficiently large, $J_2 > 0$ and $\theta_h(z) = \pi/2$ is a solution locally minimizing the free energy and therefore stable.

Together with the numerical results, we can conclude that in the presence of a strong electric field ($|\mathcal{F}|$ sufficiently large), $\theta_v(z) = 0$ is a stable solution while $\theta_h(z) = \pi/2$ is unstable. If stronger anchoring is imposed on the boundaries, then a larger value of $|\mathcal{F}|$ is needed for $\theta_v(z) = 0$ to become stable. In addition, in the presence of a weak electric field ($|\mathcal{F}|$ sufficiently small), and \mathcal{A} sufficiently large, the director solution $\theta_v(z) = 0$ is an unstable solution while $\theta_h(z) = \pi/2$ is stable. We observed numerically that in the presence of weak anchoring, the saturation threshold increased with \mathcal{A} and Υ and although we cannot arrive to the same conclusion

analytically, we observe that the sign of J_2 depends heavily on the anchoring and electric field strength, indicating that the stability of the solutions depends strongly on the parameters \mathcal{A}, \mathcal{F} .

2. Linear stability analysis

We now use LSA to determine if the director solutions $\theta_v(z) = 0$ and $\theta_h(z) = \pi/2$ pertaining to a system with weak anchoring ($\mathcal{A}_{\{0,1\}} = 5.0$) are stable or unstable. We consider planar anchoring angles $\alpha_0 = \alpha_1 = \pi/2$ and various electric field strengths, always keeping $\Upsilon = 1$. We approach the problem as follows: consider a perturbation of the steady-state solution θ_0 of the following form:

$$\theta = \theta_0 + \varepsilon \omega(z, t), \quad (\text{A10})$$

where $\varepsilon \ll 1$. Substituting Eq. (A10) into Eqs. (8) and retaining only the order ε terms, we obtain the following linear system:

$$\begin{aligned} \tilde{v} \omega_t(z, t) &= \omega_{zz}(z, t) - 2\mathcal{D} \cos 2\theta_0 \omega(z, t), \\ \tilde{v} \omega_t(0, t) &= \omega_z(0, t) \\ &\quad + [-\mathcal{A}_0 \cos 2(\theta_0 - \alpha_0) + \mathcal{F} \cos 2\theta_0] \omega(0, t), \\ -\tilde{v} \omega_t(1, t) &= \omega_z(1, t) \\ &\quad + [\mathcal{A}_1 \cos 2(\theta_0 - \alpha_1) + \mathcal{F} \cos 2\theta_0] \omega(1, t). \end{aligned} \quad (\text{A11})$$

We solve the linear boundary value problem given by Eqs. (A11) for $\theta_0 = \theta_{v,h}(z) = 0, \pi/2$ and determine whether perturbations to each solution $\theta_0(z)$ grow or decay in time. Specifically, we look for solutions of the following form:

$$\omega_1(z, t) = e^{(k^2 - 2\mathcal{D} \cos 2\theta_0)t} [A \cosh kz + B \sinh kz], \quad (\text{A12})$$

$$\omega_2(z, t) = e^{(-k^2 - 2\mathcal{D} \cos 2\theta_0)t} [A \cos kz + B \sin kz]. \quad (\text{A13})$$

Each solution $\omega_i(z, t)$, $i = 1, 2$, satisfies the linear system given by Eq. (A11) provided that the coefficients A and B are chosen to satisfy the boundary conditions. We now consider each case in detail.

a. Perturbation of hyperbolic type, Eq. (A12)

To obtain a nontrivial solution of type (A12), we need to solve the following expression:

$$\begin{aligned} D_1 \equiv \text{Det}(\omega_1) &= [k^2 - 2\mathcal{D} \cos 2\theta_0 + \mathcal{A}_0 \cos 2(\theta_0 - \alpha_0) \\ &\quad - \mathcal{F} \cos 2\theta_0] \{ (k^2 - 2\mathcal{D} \cos 2\theta_0) \tanh(k) \\ &\quad + k + [\mathcal{A}_1 + \cos 2(\theta_0 - \alpha_1) + \mathcal{F} \cos 2\theta_0] \tanh(k) \} \\ &\quad + k [(k^2 - 2\mathcal{D} \cos 2\theta_0 + \mathcal{A}_1 \cos 2(\theta_0 - \alpha_1) \\ &\quad + \mathcal{F} \cos 2\theta_0 + k \tanh(k))] = 0 \end{aligned} \quad (\text{A14})$$

and find nonzero values of k that correspond to nontrivial solutions of Eq. (A11). We find the values of k using the bisection method and observe that the evolution of $\omega_1(z, t)$ in time is driven by the exponential term $e^{(k^2 - 2\mathcal{D} \cos 2\theta_0)t}$. Specifically, if $k^2 - 2\mathcal{D} \cos 2\theta_0 < 0$ for nonzero values of k that satisfy Eq. (A14), then the perturbation $\omega_1(z, t) \rightarrow 0$ as $t \rightarrow \infty$. Similarly, if $k^2 - 2\mathcal{D} \cos 2\theta_0 > 0$ for nonzero k

TABLE I. Evolution of $\omega_1(z, t) = e^{(k^2 - 2D \cos 2\theta_0)t} [A \cosh kz + B \sinh kz]$ for $\theta_0 = 0$ and $\pi/2$ for weak anchoring $\mathcal{A}_0 = \mathcal{A}_1 = 5$ and different electric field strengths, always with $\Upsilon = 1$.

$\theta_0(z)$	α_0, α_1	$\omega_1(z, t) = e^{(k^2 - 2D \cos 2\theta_0)t} [A \cosh kz + B \sinh kz]$			$\lim_{t \rightarrow \infty} \omega_1(z, t)$
		\mathcal{F}	\mathcal{D}	k	
0	$\pi/2, \pi/2$	1	1	$\pm 1.9538, \pm 2.3815$	∞, ∞
$\pi/2$	$\pi/2, \pi/2$	1	1	0	N/A
0	$\pi/2, \pi/2$	5	25	$\pm 6.5887, \pm 7.2620$	0, ∞
$\pi/2$	$\pi/2, \pi/2$	5	25	0	N/A
0	$\pi/2, \pi/2$	9	81	$\pm 12.0797, \pm 12.7759$	0, ∞
$\pi/2$	$\pi/2, \pi/2$	9	81	0	N/A
0	$\pi/2, \pi/2$	20	400	$\pm 27.5223, \pm 28.2271$	0, 0
$\pi/2$	$\pi/2, \pi/2$	20	400	0	N/A

satisfying Eq. (A14), then $\omega_1(z, t) \rightarrow \infty$ as $t \rightarrow \infty$. Note that when $k = 0$, the perturbation $\omega_1(z, t) = A e^{(-2D \cos 2\theta_0)t}$ does not satisfy the boundary value problem given by Eq. (A11) unless the coefficient A is zero, giving the zero solution. Before we can draw any conclusions about the stability of each director solution, we must also consider perturbations given by Eq. (A13).

b. Perturbation of oscillatory type, Eq. (A13)

Similarly, to obtain a nonzero solution for Eq. (A13), we need to solve the following expression:

$$\begin{aligned}
 D_2 \equiv \text{Det}(\omega_2) &= [k^2 + 2D \cos 2\theta_0 - \mathcal{A}_0 \cos 2(\theta_0 - \alpha_0) \\
 &+ \mathcal{F} \cos 2\theta_0] \{ [k^2 + 2D \cos 2\theta_0 \\
 &- \mathcal{A}_1 \cos 2(\theta_0 - \alpha_1) + \mathcal{F} \cos 2\theta_0] \sin(k) \\
 &- k \cos(k) \} - k \{ [k^2 + 2D \cos 2\theta_0 - \mathcal{A}_1 \cos 2(\theta_0 - \alpha_1) \\
 &+ \mathcal{F} \cos 2\theta_0] \cos(k) + k \sin(k) \} = 0. \quad (\text{A15})
 \end{aligned}$$

Again, Eq. (A15) is solved numerically using the bisection method to determine the nonzero values of k that allow for nontrivial solutions for Eq. (A11). Now, the evolution of $\omega_2(z, t)$

in time is driven by the exponential term $e^{(-k^2 - 2D \cos 2\theta_0)t}$. If $-k^2 - 2D \cos 2\theta_0 > 0$ for nonzero values of k that satisfy Eq. (A15), then the perturbation $\omega_2(z, t) \rightarrow \infty$ as $t \rightarrow \infty$. Similarly, if $-k^2 - 2D \cos 2\theta_0 < 0$ then the perturbation $\omega_2(z, t) \rightarrow 0$ as $t \rightarrow \infty$.

c. Stability of solutions $\theta_v(z) = 0$ and $\theta_h(z) = \pi/2$ using linear stability analysis

We determine the stability of the steady solutions $\theta_v(z) = 0$ and $\theta_h(z) = \pi/2$ by combining the results obtained for both perturbations $\omega_i(z, t), i = 1, 2$, as follows: if both exponents in $\omega_i(z, t)$ are negative (i.e., $k^2 - 2D \cos 2\theta_0 < 0$ and $-k^2 - 2D \cos 2\theta_0 < 0$) for nontrivial values of k that satisfy Eqs. (A14) and (A15), respectively, then the perturbations $\omega_i(z, t)$ decay in time leading to a stable steady state $\theta(z)$. If at least one expression is positive, then at least one perturbation $\omega_i(z, t)$ grows in time leading to an unstable steady state. We now present two tables that display the values of k that satisfy Eq. (A11) for each perturbation $\omega_i(z, t), i = 1, 2$. In addition, we present the evolution of each perturbation as $t \rightarrow \infty$ to

TABLE II. Evolution of $\omega_2(z, t) = e^{(-k^2 - 2D \cos 2\theta_0)t} [A \cos kz + B \sin kz]$ for $\theta_0 = 0$ and $\theta_0 = \pi/2$ for weak anchoring $\mathcal{A}_0 = \mathcal{A}_1 = 5$ and different electric field strengths, with $\Upsilon = 1$.

$\theta_0(z)$	α_0, α_1	$\omega_2(z, t) = e^{(-k^2 - 2D \cos 2\theta_0)t} [A \cos kz + B \sin kz]$			$\lim_{t \rightarrow \infty} \omega_2(z, t)$
		\mathcal{F}	\mathcal{D}	k	
0	$\pi/2, \pi/2$	1	1	$\pm 3.4842 \pm 6.5394,$ others	0, 0, 0
$\pi/2$	$\pi/2, \pi/2$	1	1	$\pm 2.0930, \pm 2.8918,$ others	0, 0, 0
0	$\pi/2, \pi/2$	5	25	$\pm 3.2333, \pm 6.4098,$ others	0, 0, 0
$\pi/2$	$\pi/2, \pi/2$	5	25	$\pm 3.0228, \pm 5.8396,$ others	$\infty, \infty, 0$
0	$\pi/2, \pi/2$	9	81	$\pm 13.1757, \pm 6.3418,$ others	0, 0, 0
$\pi/2$	$\pi/2, \pi/2$	9	81	$\pm 3.1704, \pm 6.1932,$ others	$\infty, \infty, 0$
0	$\pi/2, \pi/2$	20	400	$\pm 3.1491, \pm 6.2977,$ others	0, 0, 0
$\pi/2$	$\pi/2, \pi/2$	20	400	$\pm 3.1339, \pm 6.26723,$ others	$\infty, \infty, 0$

determine the stability of each director solutions: $\theta_v(z) = 0$ and $\theta_h(z) = \pi/2$ for different electric field strengths.

Based on our LSA results shown in Tables I and II, for parameter values $\mathcal{F} = \mathcal{D} = 1$ and symmetric anchoring conditions, we conclude that $\theta_v(z) = 0$ is an unstable steady state and $\theta_h(z, t) = \pi/2$ a stable state. As we increase the electric field strength to $\mathcal{F} = 5$, $\mathcal{D} = 25$ and $\mathcal{F} = 9$, $\mathcal{D} = 81$, we observe that neither $\theta_v(z) = 0$ nor $\theta_h(z) = \pi/2$ are stable. In fact, our numerical results show that $\theta_n(z)$ is the stable solution in this case. Moreover, for a higher electric field strength $\mathcal{F} = 20$ and $\mathcal{D} = 400$, LSA shows that $\theta_v(z) = 0$ is a stable state while $\theta_h(z)$ is unstable. Note that

for all choices of \mathcal{F} , \mathcal{D} used here, the material parameter $\Upsilon = 1$.

Although these analytical approaches are very useful to validate our numerical results, they have their limitations. In the case of the calculus of variations method, we are able to draw conclusions only in the limiting cases where $|\mathcal{F}|$ is small or large compared to the anchoring strength $\mathcal{A}_{\{0,1\}}$. When using LSA, we are able to linearize only around known solutions, namely, $\theta(z) = 0, \pi/2$ and for symmetric anchoring conditions only. We still rely on our numerical investigation to determine the stability of the nontrivial steady state as well as asymmetric boundary conditions.

-
- [1] K. Blankenbach, L.-C. Chien, S.-D. Lee, and M. H. Wu (eds.), Proc. SPIE **7956** (2011).
- [2] P. G. De Gennes and J. Prost, *The Physics of Liquid Crystals* (Oxford University Press, New York, 1995).
- [3] R. B. Meyer, *Phys. Rev. Lett.* **22**, 918 (1969).
- [4] A. Buka and N. Éber, *Flexoelectricity in Liquid Crystals: Theory, Experiments and Applications* (Imperial College Press, London, 2013).
- [5] V. Fréedericksz and A. Repiewa, *Z. Phys.* **42**, 532 (1927).
- [6] C. Brown and N. Mottram, *Phys. Rev. E* **68**, 031702 (2003).
- [7] A. Derzhanski, A. G. Petrov, and M. D. Mitov, *J. Phys. (Paris)* **39**, 273 (1978).
- [8] G. Napoli, *J. Phys. A: Math. Gen.* **39**, 11 (2006).
- [9] F. P. Da Costa, M. Grinfeld, N. J. Mottram, and J. T. Pinto, *J. Differ. Equations* **246**, 2590 (2009).
- [10] L. J. Cummings and G. Richardson, *Eur. J. Appl. Math* **17**, 435 (2006).
- [11] L. J. Cummings, C. Cai, and L. Kondic, *J. Eng. Math.* **80**, 21 (2013).
- [12] L. J. Cummings, C. Cai, and L. Kondic, *Phys. Rev. E* **88**, 012509 (2013).
- [13] L. J. Cummings, E. Mema, C. Cai, and L. Kondic, *Phys. Rev. E* **90**, 012503 (2014).
- [14] I. W. Stewart, *The Static and Dynamic Continuum Theory of Liquid Crystals* (Taylor & Francis, London, 2004).
- [15] S. Chandrasekhar, *Liquid Crystals* (Cambridge University Press, Cambridge, 2007).
- [16] L. M. Blinov and V. Chigrinov, *Electrooptic Effects in Liquid Crystal Materials* (Springer, New York, 1994).
- [17] J. Prost and P. Pershan, *J. Appl. Phys.* **47**, 2298 (1976).
- [18] L. Blinov, M. Barnik, H. Ohoka, M. Ozaki, N. Shtykov, and K. Yoshino, *Eur. Phys. J. E* **4**, 183 (2001).
- [19] L. Blinov, M. Barnik, H. Ohoka, M. Ozaki, and K. Yoshino, *Jpn. J. Appl. Phys.* **40**, 5011 (2001).
- [20] L. Jinwei, Z. Suhua, Y. Yuying, A. Hailong, Z. Zhendong, and Y. Guochen, *Liq. Cryst.* **34**, 1425 (2007).
- [21] A. Zakharov and R. Dong, *Phys. Rev. E* **64**, 042701 (2001).
- [22] A. Rapini and M. Papoular, *J. Phys. Colloq. (Paris)* **30**, C4-54 (1969).
- [23] P. J. Kedney and F. M. Leslie, *Liq. Cryst.* **24**, 613 (1998).
- [24] A. J. Davidson and N. J. Mottram, *Phys. Rev. E* **65**, 051710 (2002).
- [25] S. V. Pasechnik, V. G. Chigrinov, and D. V. Shmeliova, *Liquid Crystals: Viscous and Elastic Properties* (Wiley-VCH, Weinheim, 2009).
- [26] K. E. Atkinson, *An Introduction to Numerical Analysis* (John Wiley & Sons, Inc., New York, 1989).
- [27] D.-K. Yang and S.-T. Wu, *Fundamentals of Liquid Crystal Devices* (Wiley, Chichester, 2014).
- [28] M. C. Choi, Y. Kim, and C. S. Ha, *Prog. Polym. Sci.* **33**, 581 (2008).
- [29] J. S. Gwag, J.-H. Kim, M. Yoneya, and H. Yokoyama, *Appl. Phys. Lett.* **92**, 153110 (2008).